IMPROVING THE PERFORMANCE OF (HgCdTe) PHOTODETECTORS OF INFRARED SEARCH AND TRACK SYSTEMS FOR (3-5 µm) BAND

Fathi Mohmed Al-Gomati and Abdul hakim M. Hamouda
Physics Dep. Faculty of Arts and Science, University of Gharyan, Mizda,

المستخلص :

يتطلب تصميم كواشف الأشعة تحت الحمراء بكفاءة عالية والتي تستخدم في أنظمة كشف وتتبع الأشعة تحت الحمراء (IRST) دراسة عدة متغيرات (بارامترات) و تحسينها. و قد تم اختيار الكاشف ($Hg_{1-xcd}Cd_{xcd}Te$) حيث يعتبر هذا الكاشف الأكثر شيوعا و ملائمة في تطبيقات هذه الأنظمة في النافذة (3−5μm) .

إن الهدف من هذه الدراسة هوالعمل على تطوير و تحسين فعالية هذا النوع من الكواشف و ذلك بدراسة وتحسين خواصه الكهربائية والبصرية، ولهذا الغرض فقد تم استخدام برنامج (MATLAB software) لمعرفة مدى تأثير قيم (x_{cd}) على الخواص الكهربائية والضوئية للكاشف عند قيم مختلفة لدرجة الحرارة.

تم تحديد القيم المناسبة لـ (x_{cd}) التي تكون فيها استجابة وحساسية الكاشف ملائمة في النطاق (3−5μm) للأشعة تحت الحمراء، ومن خلال النتائج تبين أن الاستجابة العظمى لهذا النوع من الكواشف تكون محققة في المدى ($0.40 > x_{cd} > 0.28$).

ABSTRACT

The design of high performance photodetectors for infrared search and track (IRST) systems requires a study of the various parameters of the photodetectors and improve these parameters by modelling and optimizing of specific figures of merit of photodetectors for IR system. As the most often used and the most convenient photodetector material for (IRST) applications in 3-5µm, window mercury cadmium telluride, ($Hg_{1-x}Cd_xTe$) was chosen.

The objective of this study is to investigate the performance improvement method of (HgCdTe) infrared photodetectors for (3-5µm) band. In order to improve their electrical and optical parameters their figures of merit The

MATLAB software is applied and the approaches to their optimization have been investigated.

The influence of different important parameters has been investigated, i.e. the operating temperature, composition (x_{cd}), etc. From our results it was found that the maximum responsivity of such type of photodetectors is fulfilled at (3-5μm) band, when the value of x_{cd} lies in the range of ($0.40 > x_{cd} > 0.28$).

1. INTRODUCTION

Infrared photodetector is the heart of an infrared search and track (IRST) systems because it plays a key role in determining system-level parameters including spectral operating band, sensitivity, and resolution. Mercury-Cadmium-Telluride (HgCdTe) also referred to as MCT is the dominant material for development of high sensitivity infrared photodetectors for military applications, medical imaging, and surveillance, and many other applications. The adjustable energy gap of (HgCdTe) with sensitivity spanning from short wavelength (SWIR) to very long wavelength (VLWIR) infrared windows enables it for tremendous potential applications to be realized using advance material growth methods and different (HgCdTe) photodetectors design. (HgCdTe) can be used for photodetectors operated at various modes, and can be optimized for operation at the extremely wide range of the IR spectrum (1–50μm) and at temperatures ranging from that of liquid helium (*4 K)* to room temperature.

2. THE PRINCIPAL COMPONENTS OF IRST SYSTEM.

Infra-Red Search and Tracking (IRST) System sensor is used for battlefield night vision, surveillance of unlit area, and fire detection within smoke-filled space onboard ships. The typical sensor of (IRTS) provides a visual representation of an object at night or under poor lighting conditions. The principal components of an IR tracking system are:

1. Radiation sources (Target and background)
2. Atmospheric window
3. Optics
4. Detector and cooler system if required
5. Electronics (signal and image processing systems)
6. Display.

Typical scenario for IRST system is shown in figure (2.1).

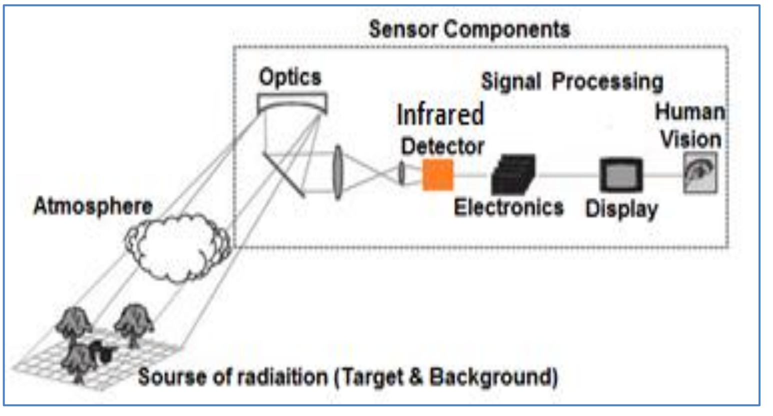

Figure (2.1) Typical scenario of an IRTS system [1].

2.1 SOURCES OF RADIATIATON

The first component in the (IRST) system is the objects that are viewed by the sensor. Objects, as seen by sensors, include targets and backgrounds. Target characterization is very important part of the overall sensor analysis and design process. Sensor band selection for a scenario begins with the targets and background. The radiation emitted by the sun, which is considered to be a blackbody approximately at 5800 K, reaches its maximum in the visible region of the spectrum. Therefore, the sun is in tune with human eyes. On the other hand, subjects at temperature 900 K emit almost entirely in the (IR) band and thus are not visible to the eye unless they reflect light coming from other sources. A target-background difference in existence (or emittance) must be present in the band of interest.

2.2 ATMOSPHERIC WINDOW

From the standpoint of the designer and user of the (IRST) systems, it is unfortunate that most of the systems view their targets through the earth's atmosphere. Before it reaches the IR receiver unit, the target radiation flux has been changed due to numerous processes. In calculating the optical transmission from an object to a sensor, there are three primary processes that affect the radiation: scattering, absorption, and turbulence. The effect of these three factors is both a reduction in the amplitude of the signal that reaches the sensor from the target and an atmospheric blurring of the image. Figure (2.2) is a plot of the transmission through (6000 ft) of air as a function of wavelength. Specific absorption bands of carbon dioxide, oxygen, and water molecules are indicated which restricts atmospheric transmission to two windows at (8-14μm) and (3-5μm).

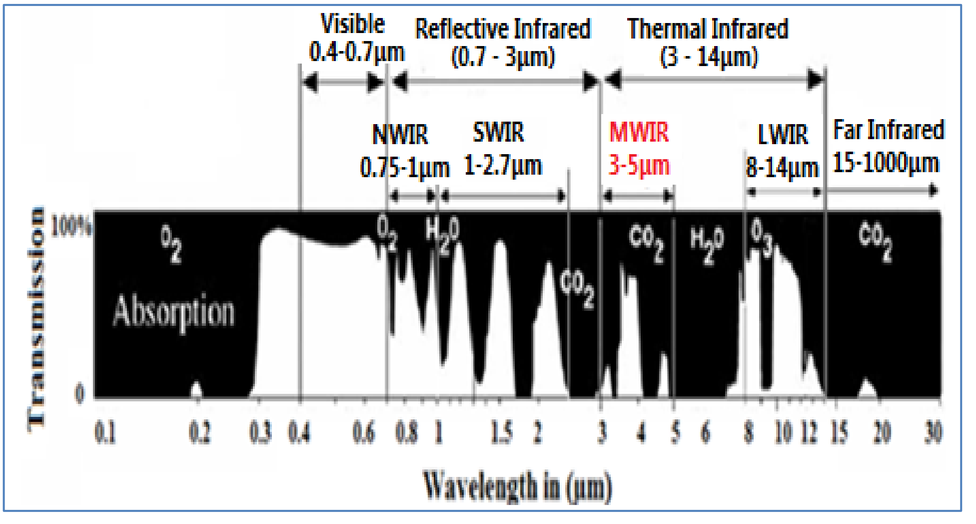

Figure (2.2) Typical atmospheric transmission as a function of wavelength.

2.3 OPTICS SYSTEM

In the design of the (IRST) optics system, it is important to understand the limitations that optical components introduce in the overall system parameters. Among the parameters that the optics defines are spatial and spectral properties of the sensor system, field of view (FOV), and resolution. All elements are considered to be centered; that is, the centers of curvature of each surface all lies on the same straight line called the optical axis. The IR-transmitting materials potentially available for use as windows and lenses are shown in Figure (2.3).

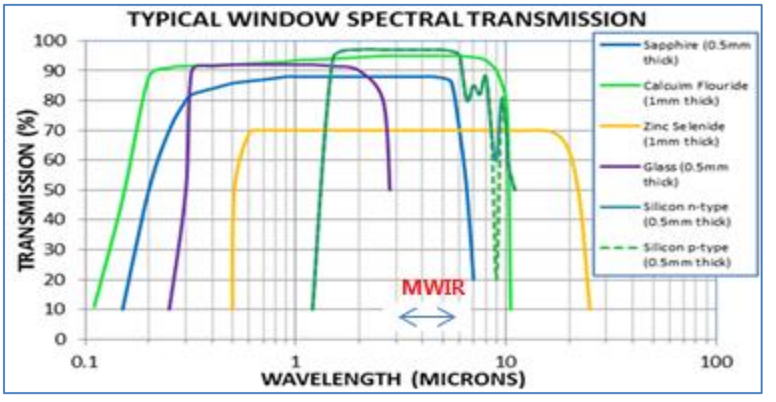

Figure (2.3) Infrared materials, transmission range [2].

2.4 IR DETECTORS

The detector component in sensors of the IRST systems plays a key role in determining system-level parameters including sensitivity, resolution, and spectral operating band. The spectral response is determined by the detector material characteristics and the operating temperature. The detector sensitivity is a function of material (i.e., band gap), detector size, bandwidth, wavelength, and shielding.

There are two general classes [3, 4] of detectors: *photon* and *thermal* detectors. Photon detectors include photoconductors (PC), photovoltaic (PV), and photo-emissive detectors, they exhibit both a good signal−to−noise performance and a very fast response. But to achieve this, the photon IR detectors require cryogenic cooling. Thermal detector materials have at least one inherent electrical property that changes with temperature. This temperature-related property is measured electrically to determine the power on the detector [5]. The detector material most employed in IR system is Mercury Cadmium Telluride (HgCdTe). The adjustable bandgap of (HgCdTe) photodetectors with sensitivity spanning from (SWIR) to (VLWIR) infrared bands enables it for tremendous potential applications to be realized using advance material growth methods and different detectors design.

2.5 ELECTRONICS

The function of electronics is to transform the output of the IR detector into a signal that can be processed or viewed. This transformation must be accomplished with minimal degradation of system performance. Issues of primary importance are high gain, low output impedance, large dynamic range, low noise and good linearity. Figure (2.4) shows an example of the basic operation circuit for MCT photoconductive detectors.

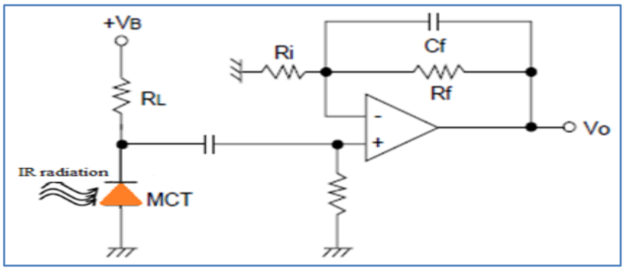

Figure (2.4) Basic operation circuit for MCT photoconductive detectors [6].

This type of circuit is used for low output impedance, nominal-input impedance, and high-gain. However, there is a signal inversion (i.e., the signals are 180 deg. out of phase) from the detector voltage to the output voltage [7].

2.6 IMAGE PROCESSING

The principal IRST technical challenges are tracking subpixel targets in moving clutter and additive noise and with a bipolar format, allowing targets to be below or above the immediate background level. In general, targets may exhibit both negative and positive contrasts with respect to the background.

Discrimination is the process of differentiating between target and (false target) background clutter. In IRST systems discrimination may be implemented through differences in signal frequency or amplitude, motion, spatial characteristics, or received IR spectrum. Differences can be detected in ways ranging from simple thresholding to sophisticated space-time correlations. All are generally employed in modern IRST systems [8].

2.7 DISPLAYS, HUMAN PERCEPTION

Displays are the interface between the IR sensor and the human vision system. The display converts the electrical signal from the IR sensor to a visible signal that is subsequently presented to the viewer. Occasionally, systems are designed where humans do not interpret the data, so displays are not required. Imaging system with automatic target trackers are a good example. Various levels of human interpretation of imagery are seen in the targeting community. One example that is increasingly successful and gaining popularity is the targeting sensor coupled to a computerized automatic target recognizer (ATR), automatic target cueing (ATC) system, or aided target recognizer (AiTR).

3. INFRARED SPP.

Semiconductor Photoconductive Photodetectors (SPP) works on the principle of change in electrical conductivity when illuminated by infrared radiation. When a semiconductor is illuminated by IR radiation, the concentration of carriers is increased by optical absorption by excitation over the band gap. This increase in the conductivity is the basis of photoconductive detection. The principle of photoconductive detector detection is shown in Figure (3.1).

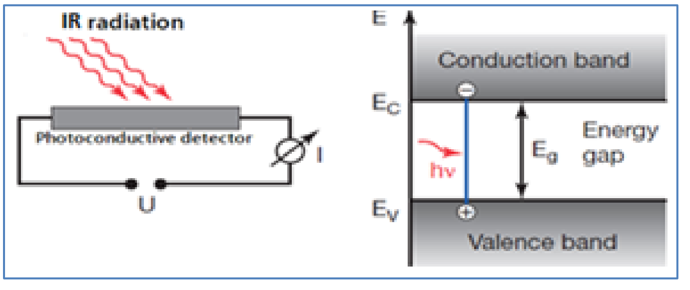

Figure (3.1) The incident radiation leads to charge carriers within the conduction and valence bands of the semiconductor materials.

In view of the fact that the atmospheric transmission has windows in the SWIR (1-2.7 µm), MWIR (3-5 µm), and in the LWlR (8-14 µm) bands, so we are interested in IR detection in these bands, the energy gap of the semiconductor should correspond to the energies of photons in these regions of the spectra. The three window regions correspond to photon energies in the range of (0.50-1.24 eV), (0.2-0.41 eV) and (0.09-0.15 eV), respectively.

The detector material most employed in IR system is Mercury Cadmium Telluride ($Hg_{1-xcd}Cd_{xcd}Te$). The band gap of this type of photodetectors can be varied continuously from 0 to 1.6 eV by varying x_{cd}.

3.1 IRSP PARAMETERS AND FIGURES OF MERIT

In order to specify and compare the performance of various photodetectors it is necessary to define certain figures of merit to describe this conversion efficiency and the magnitude of the signal-to-noise ratio of the photodetector in terms of the incident radiation power.

3.1.1 Quantum Efficiency (η)

The quantum efficiency ($0 \leq \eta \leq 1$) of a photodetector is defined as the probability that a single photon incident on the device generates a photo-carrier pair that contributes to the detector current. When many photons are incident, η is the ratio of the flux of generated electron-hole pairs that contribute to the photodetector current to the flux of incident photons [9].

$$\eta = \frac{i_p \, h\nu}{q \, P_o} \quad \text{...................................... (3.1)}$$

Where: i_p: is the photocurrent, q : is the carrier charge, P_o: is the optical power, h: Plank' s constant, and v : incident photon frequency.

3.1.2 Responsivity (R)

One of the most important properties of any photodetector is its responsivity (R), which defined as the photodetector output signal per unit incident radiation power. The responsivity (R) relates the electric current flowing in the device to the incident optical power.

$$R = \frac{\eta e}{h\nu} = \eta \frac{\lambda_o(\mu\text{m})}{1.24} \quad \text{.............................. (3.2)}$$

The responsivity can be degraded if the photodetector is presented with an excessively large optical power. This condition, which is called photodetector saturation, limits the photodetector's linear dynamic range, which is the range over which it responds linearly with the incident optical power [9].

3.1.3 Noise Equivalent Power (NEP)

Although the responsivity effectively defines the sensitivity of a device it gives no indication of the minimum radiant flux that can be detected. This minimum detectable flux is defined as the incident radiation power required to producing an output signal (V_s) equal to the internal noise level of photodetector (V_n), in other words, a signal-to-noise ratio of unit, and is known as the noise equivalent power.

$$NEP = \frac{V_n}{R} \quad \text{.. (3.3)}$$

3.1.4 Detectivity (D)

It can be seen that the higher the performance of a photodetector the lower the value of noise equivalent power (NEP). This is described by the photodetector detectivity as:

$$D = \frac{1}{NEP} \quad [\ \text{Hz}^{1/2}/\text{W}\ ] \quad \text{.............................. (3.4)}$$

When the detectivity is used to characterize a photodetector it is necessary to specify the wavelength of the incident IR radiation, the photodetector temperature, any bias current applied to the device, the chopping frequency, the area of the photodetector and the bandwidth of the amplifier used to measure the photodetector noise.

3.1.5 Specific Detectivity (D*)

The detectivity is not an ideal parameter for comparing different detectors as it varies inversely as the square root of both the bandwidth (Δf) and the sensitive area. Hence the specific detectivity or D^* (D-star) measured in [$cmHz^{1/2}/W$] has been introduced such that:

$$D^* = \frac{\sqrt{A\Delta f}}{NEP} \quad \text{..} \quad (3.5)$$

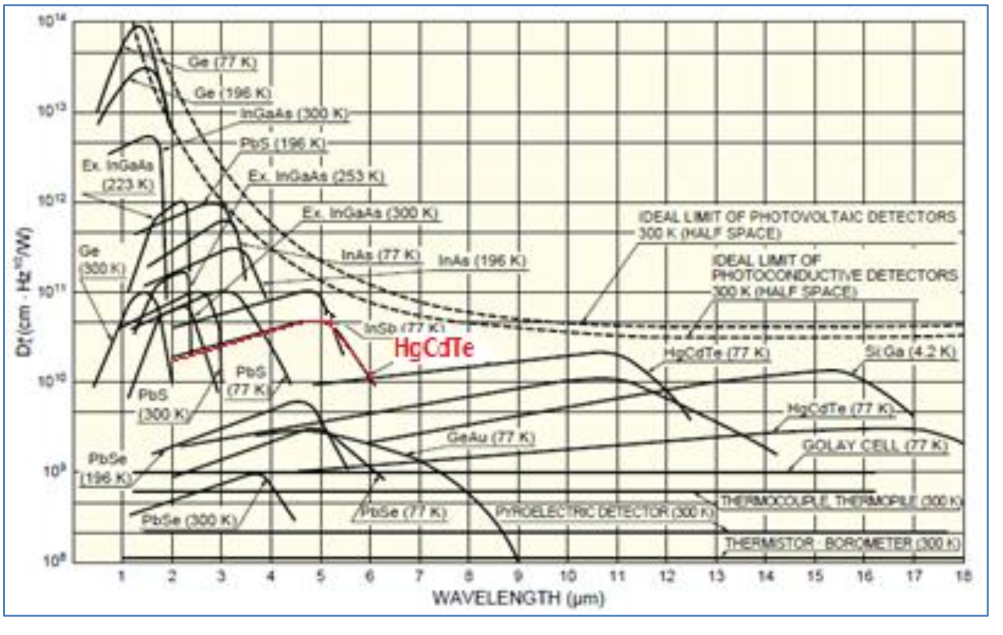

Figure (3.2) Spectral response characteristics of various infrared detectors [10].

4. BASIC PARAMETERS OF MCT PHOTOCONDUCTIVE.

There are some important parameters of MCT photoconductive such as Bandgap(E_g), Intrinsic Carrier Concentration (n_i) , Electron Effective Mass(m_n^*) , Electron mobility (μ_n) , Hole mobility (μ_p) , and Absorption coefficient (α) . These parameters can be briefly illustrated as follows.

- Band-Gap (BG):

There are a number of expressions, approximating E_g as a function of Cadmium molar fraction x_{cd} and temperature T are available at present. The widely used expression is due to Hansen et al [11].

$$E_g(x_{cd}, T) = -0.302 + 1.9x_{cd} + 5.35 \times 10^{-4}T(1 - 2x_{cd}) - 0.81x_{cd}^2 + 0.832x_{cd}^3 \quad \text{(4.1)}$$

- Intrinsic Carrier Concentration(ICC):

$$n_i = (5.85 - 3.82x_{cd} + 1.735 \times 10^{-3}T - 0.001364x_{cd}T) \times [10^{20}E_g^{3/4}e^{-E_g/2k_bT}] \quad \text{(4.2)}$$

- Electron Effective Mass(EEM):

$$m_n^* = \frac{m_0}{1 + 2m_0P_1^2 \frac{q}{3}\left(\frac{2\pi}{h}\right)^2\left(\frac{2}{E_g} + \frac{1}{E_g + 1}\right)} \quad \text{(4.3)}$$

Where, q : is the magnitude of the electron charge.
P_o : is the optical power .
h : Plank' s constant.
m_0 : is the electron rest mass.

- Electron Mobility(EM):

$$\mu_n = 1.46 \cdot 10^5 \left(\frac{0.14}{x_{Cd}}\right)^{7.5} \frac{1}{T^{2(0.14/x_{Cd})}} \quad \text{(4.4)}$$

- Hole Mobility(HM):

$$\mu_p = (\mu_n/100) \quad \text{(4.5)}$$

- Absorption Coefficient (AC):

$$\alpha = (1480x_{Cd} + 0.26T + 90)e^{3.915\mathrm{sgn}(E-E_g)(E-E_g)^{1/3}}$$
$$\{th[120th(10x_{Cd} - 1.5)(E - E_g)] + 1\} \quad \ldots\ldots\ \ldots\ldots\ldots\ldots(4.6)$$

5. SIMULATIONS, RESULTS AND DISCUSSION

The Detectivity (D*), Sensitivity (S), and Quantum efficiency (μ) of HgCdTe Photoconductors are calculated using the following parameters:

- Cadmium molar fraction x_{cd} =0.40, 0.32, 0.29 and, 0.28
- Detector dimensions (width = 1000 μm, length =1000 μm, thickness=0.184 μm),
- Bias voltage =1.5V, and
- Optical infrared power of illumination= 0.0001 W.

5.1 Calculation of (D*), (S), and (μ) for x_{cd} =0.40

Figure (5.1a) shows the Detectivity (D*) versus wavelength (λ), with detector temperature (T) as a parameter. The D*(λ) dependence was calculated for five different values of T, these being T1=77 K, T2=100K, T3=150 K, T4=200 K, and T5=300 K. Also, the S (λ) and η(λ) were calculated for the same previous parameter with the same constants. The range of (λ), varied from zero to 4 μm,

The results of each (D*), (S) and η(λ) against the wavelength (λ), with the detector temperature (T) are shown in figures (6.1a, b, and c) respectively.

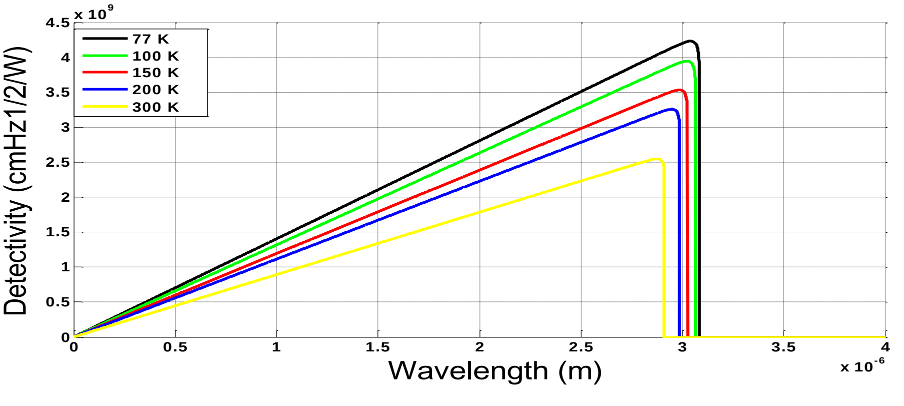

Figure (5.1a) Detectivity (D*) of MCT versus wavelength (λ) for x_{cd} =0.40

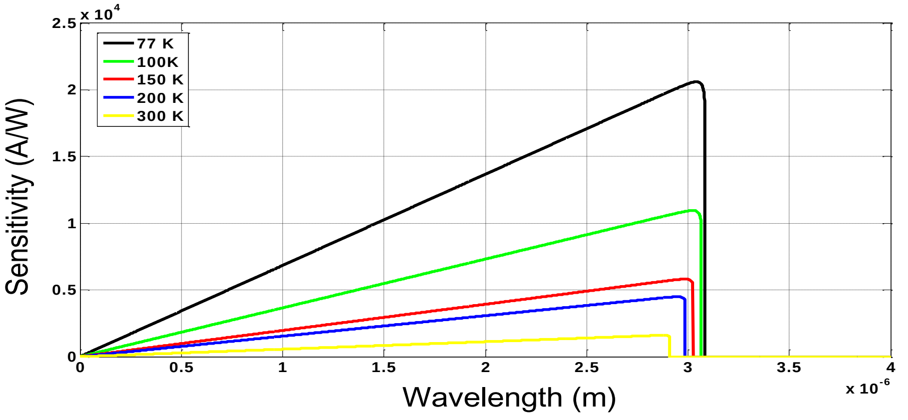

Figure (5.1b) Sensitivity (S) of MCT versus wavelength (λ) for x_{cd} =0.40

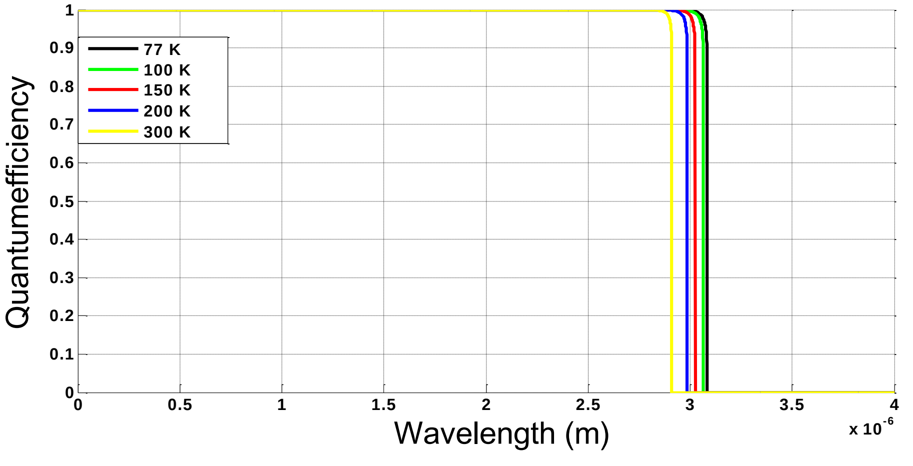

Figure (5.1c) Quantum efficiency (μ) of MCT versus wavelength (λ) for x_{cd} = 0.40

From Figure (5.1a), it can be seen that D* first rises with λ, reaching a maximum value of λ about 3.04μm at T1, 3.02μm at T2, 2.98μm at T3, 2.94μm at T4, and 2.87μm at T5, and then quickly drops with λ, reaching zero. Therefore, the values of D* lies in the range (0 - 4.23×10^{9}) (cmHz1/2/W).

Consequently, it can be seen from Figure (5.1b) that S(λ) slowly rises first with λ, reaching a maximum value of λ 3.04μm at T1, 3.02μm at T2, 2.98μm at T3, 2.94μm at T4, and 2.87μm at T5, and then quickly drops with λ, reaching zero, Moreover, it was found the values of S lies in the range (0 to 2.62×10^{4}) (A/W).

From Figure (5.1c) it was found that η(λ) reached values in the range (0 – 1). Here η starts with a maximum value (1) up to wavelength of about 2.79µm at T1, 2.78µm at T2, 2.75µm at T3, 2.73µm at T4, and 2.68µm at T5, and then quickly drops with λ if increased with T, reaching to zero.

The maximum values of (D*), (S), and (µ) of Hg0.60Cd0.40Te detector with their corresponding wavelengths, are shown in Table (5.1).

Table (5.1)						
x_{cd} **= 0.40**	Temperature (K)	77	100	150	200	300
D* (cmHz$^{1/2}$/W)	$D^*_{(\lambda max)}$	4.23×10^9	3.94×10^9	3.53×10^9	3.25×10^9	2.54×10^9
	λ_{max} (µm)	3.04	3.02	2.98	2.94	2.87
S (A/W)	$S_{(\lambda max)}$	2.62×10^4	1.09×10^4	5814	4490	1600
	λ_{max} (µm)	3.04	3.02	2.98	2.94	2.87
η	$\eta_{(\lambda max)}$	1	1	1	1	1
	λ_{max} (µm)	< 2.80	< 2.79	< 2.76	< 2.74	< 2.69

5.2 Calculation of (D*), (S), and (µ) for x_{cd} =0.32

Again the same procedure was repeated for x_{cd} =0.32 and T being at T_1=77K, T_2=100K, T_3=150K, T_4=200 K, and T_5=300 K. The results are shown in the figures (5.2a, b, and c).

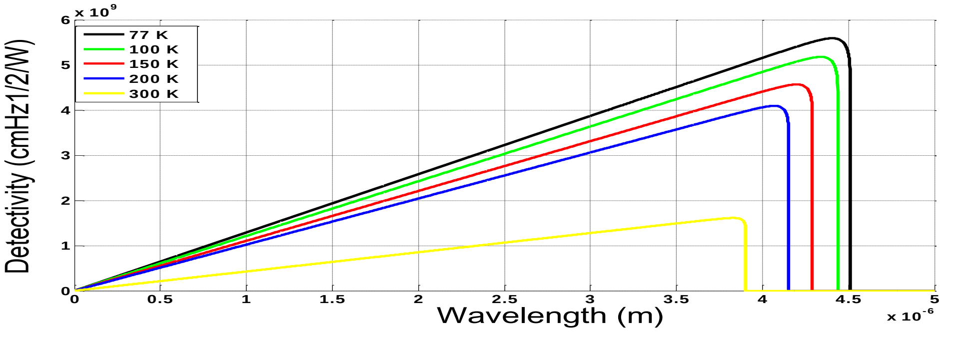

Figure (5.2a) Detectivity (D*) of MCT versus wavelength (λ) for x_{cd} =0.32

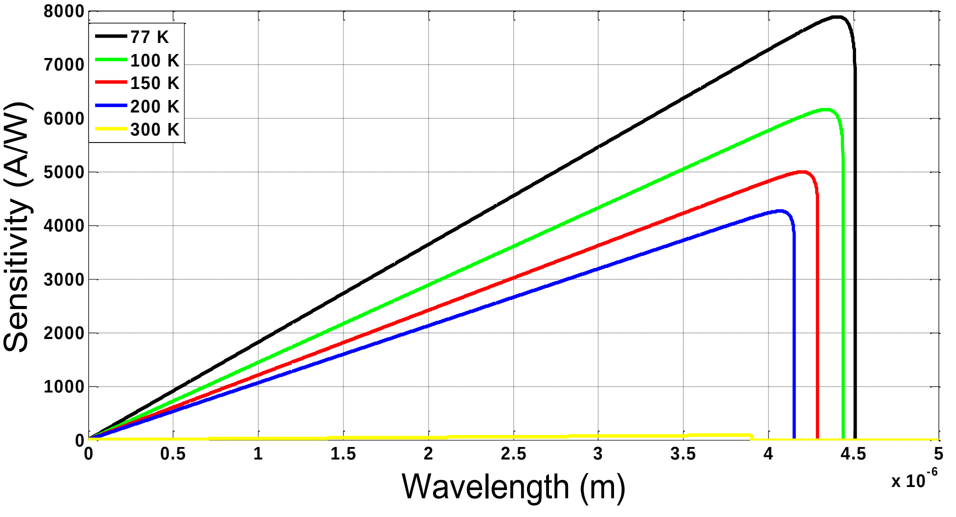

Figure (5.2b) Sensitivity (S) of MCT versus wavelength (λ) for x_{cd} = 0.32

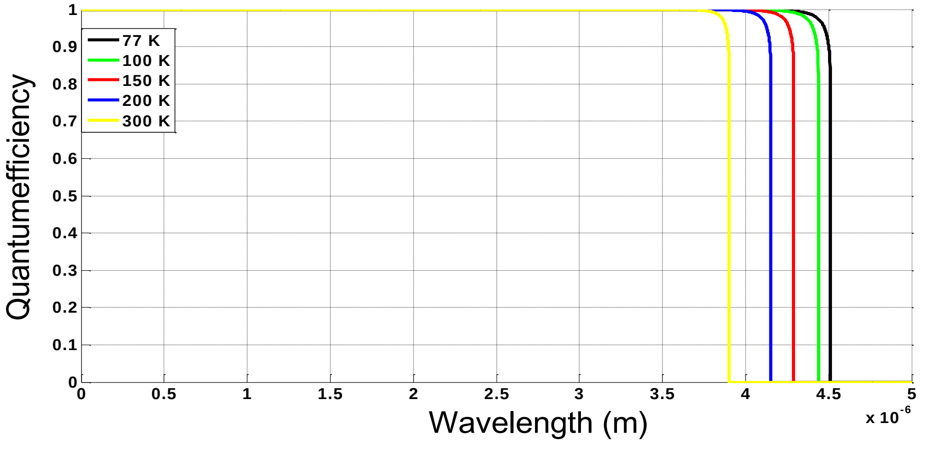

Figure (5.2c) Quantum efficiency (μ) of MCT versus wavelength (λ) for x_{cd} =0.32

The maximum values of the (D*), (S), and (μ) of $Hg_{0.68}Cd_{0.32}Te$ detector with their corresponding wavelengths are shown in Table (5.2).

Table (5.2)						
x_{cd} =0.32	Temperature (K)	77	100	150	200	300
D* ($cmHz^{1/2}/W$)	$D^*_{(\lambda max)}$	5.59×10^9	5.17×10^9	4.56×10^9	4.09×10^9	1.61×10^9
	λ_{max} (µm)	4.40	4.33	4.19	4.06	3.82
S (A/W)	$S_{(\lambda max)}$	7887	6158	4994	4263	86.51
	λ_{max} (µm)	4.40	4.33	4.19	4.06	3.82
η	$\eta_{(\lambda max)}$	1	1	1	1	1
	λ_{max} (µm)	< 3.71	< 3.67	< 3.59	< 3.52	< 3.37

5.3 Calculation of (D*), (S), and (µ) for x_{cd} =0.29

The same procedure was repeated for *xcd* = 0.29 and T being at *T1*=150K,*T2*=200K, *T3*=250 K, and *T4*= 300 K. The results of (D*), (S) and (η) are shown in the figures (5.3a, b, and c) respectively.

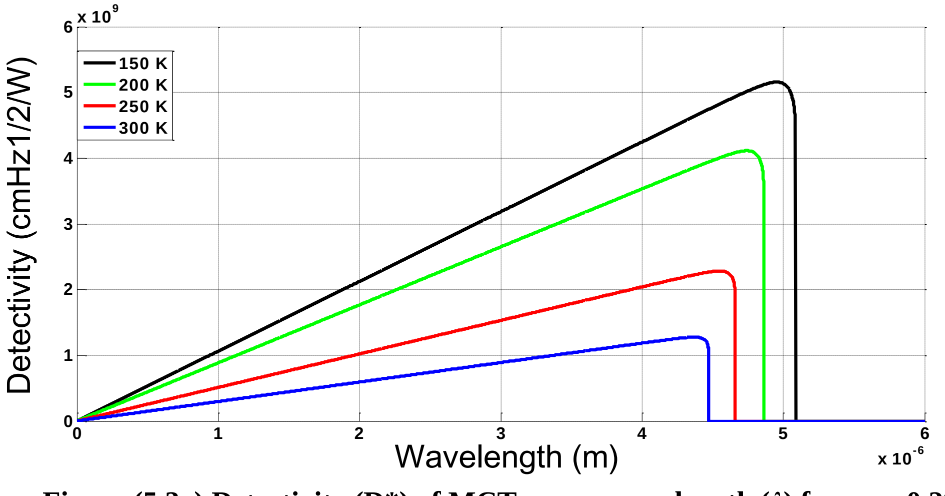

Figure (5.3a) Detectivity (D*) of MCT versus wavelength (*λ*) for x_{cd} =0.29

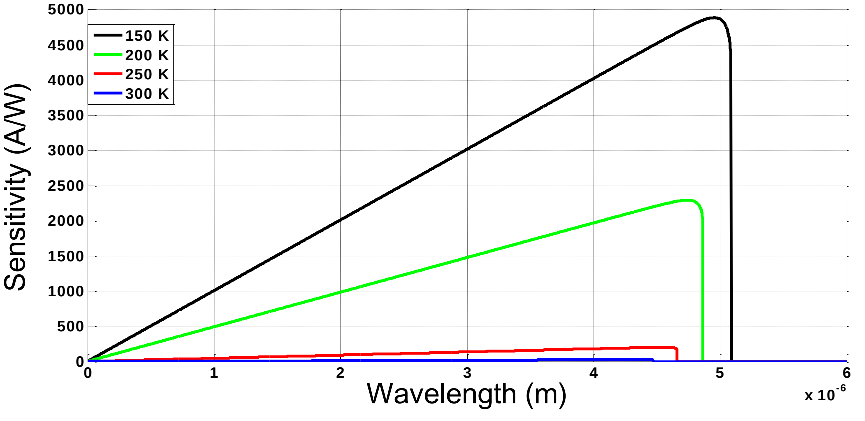

Figure (5.3b) Sensitivity (S) of MCT versus wavelength (λ) for x_{cd} =0.29

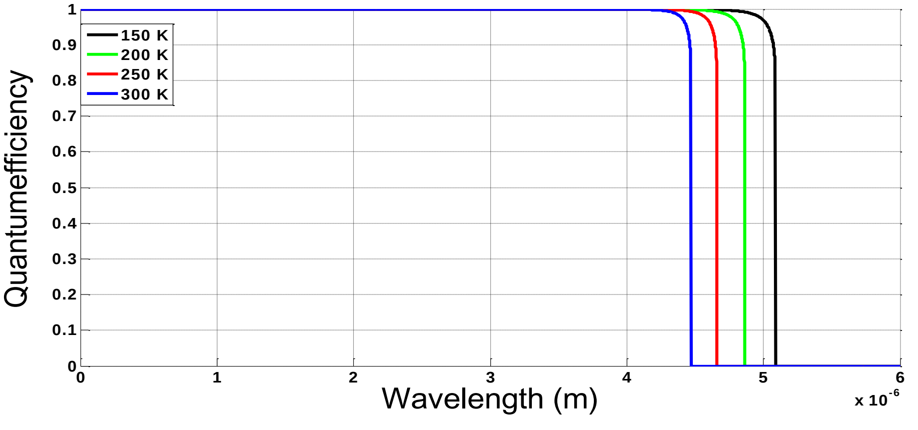

Figure (5.3c) Quantum efficiency (μ) of MCT versus wavelength (λ) for x_{cd} =0.29

The maximum values of the (D*), (S), and (μ) of $Hg_{0.71}Cd_{0.29}Te$ detector with their corresponding wavelengths, are shown in Table (5.3).

Table (5.3)					
x_{cd} =0.29	Temperature (K)	150	200	250	300
D* (cmHz$^{1/2}$/W)	$D^*_{(\lambda max)}$	5.15×10^9	4.11×10^9	2.28×10^9	1.27×10^9
	λ_{max} (μm)	4.94	4.74	4.53	4.35
S (A/W)	$S_{(\lambda max)}$	4888	2295	201.7	24.6
	λ_{max} (μm)	4.94	4.74	4.53	4.35
η	$\eta_{(\lambda max)}$	1	1	1	1
	λ_{max} (μm)	< 4.02	< 3.93	< 3.81	< 3.71

5.4 Calculation of (D*), (S), and (μ) for x_{cd} =0.28

Finally the procedure was repeated for x_{cd} = 0.28 and T being at T_1=200K, T_2=250K, and T_3=300 K. The results are shown in the figures (5.4a, b, and c).

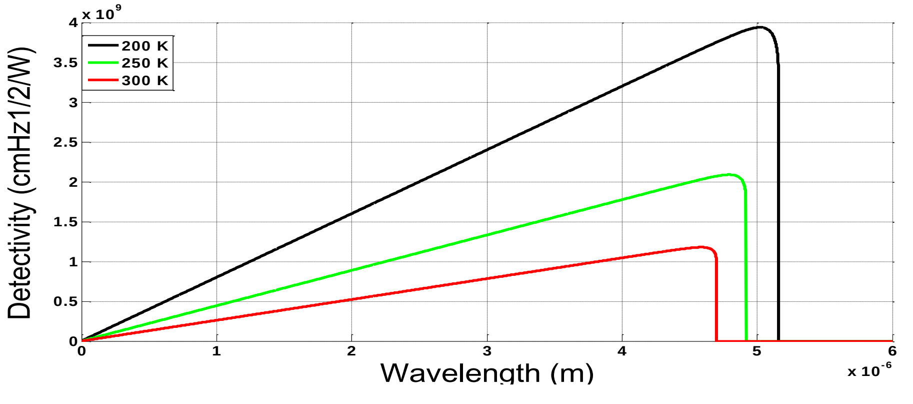

Figure (5.4a) Detectivity (D*) of MCT versus wavelength (λ) for x_{cd} =0.28

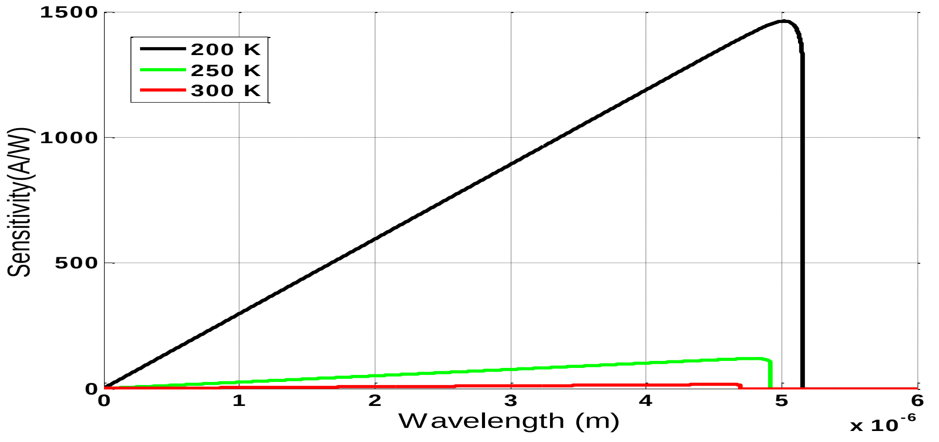

Figure (5.4b) Sensitivity (S) of MCT versus wavelength (λ) for x_{cd} =0.28

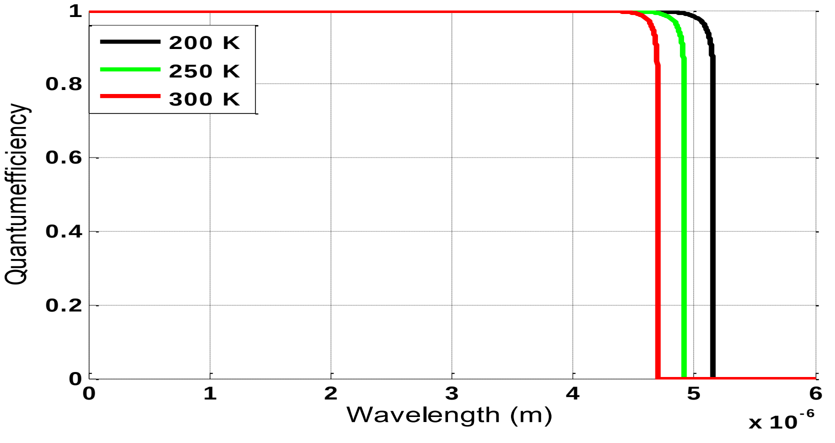

Figure (5.4c) Quantum efficiency (μ) of MCT versus wavelength (λ) for x_{cd} =0.28

The maximum values of the (D*), (S), and (μ) of $Hg_{0.72}Cd_{0.28}Te$ detector and their corresponding wavelengths are shown in Table (5.4).

Table (5.4)				
x_{cd} =0.28	Temperature (K)	200	250	300
D* (cmHz$^{1/2}$/W)	$D^*_{(\lambda max)}$	3.93×10^9	2.08×10^9	1.17×10^9
	λ_{max} (μm)	5.01	4.77	4.60
S (A/W)	$S_{(\lambda max)}$	1463	119.4	16.16
	λ_{max} (μm)	5.01	4.77	4.60
η	$\eta_{(\lambda max)}$	1	1	1
	λ_{max} (μm)	< 4.06	< 3.95	< 3.83

6. SUMMERY AND CONCLUSIONS

Based on the results presented and discussed in Section 5 several important conclusions may be drawn regarding the optimization of detectivity (D*), sensitivity (S) and quantum efficiency (η) of MCT photoconductive photodetectors for MWIR:

The very important parameter is obviously the mercury cadmium telluride composition x_{cd}. For some values of x_{cd} there is no response in the (3–5μm) band and temperatures at all, while for ($0.40 > x_{cd} > 0.28$) this response is very large. By analyzing the shape of the (D*), and (S) versus wavelength we can see that the optimum composition is the one furnishing a maximum of the (D*), and (S), and this value is the one close to the cutoff wavelength.

Lower temperatures 77 K, and 100 K are more convenient to reach high values of D*, (S), and (η), but even for higher operating temperature one can optimize the composition to obtain high detectivities and sensitivities.

For shorter wavelengths the penetration depth through the MCT photoconductive photodetectors is small because of the too large thickness and thus the (η) is too low, it gradually increases with wavelength and reaches its optimum.

REFRENCES

[1]R. G. Driggers, P. Cox, T. Edwards, "*Introduction to Infrared and Electro-Optical Systems*," Artech House, Boston-London, 1999

[2]M.E. Couture, “Challenges in IR optics,” *Proc. SPIE* 4369,649–661, 2001.

[3]Pinson, L., *Electro-Optics*, New York City, NY: Wiley, p. 103, 1985

[4]*The Photonics Dictionary*, Pittsfield, MA: Laurin Publishing Company, 1996.

[5]Dereniak, E., and G. Boreman, *Infrared Detectors and Systems*, New York City, NY: Wiley, p. 86, 1996

[6]Kudo, nakura; infrared technology (Japanese) 11, P73, 1986

[7]Ronald G. Driggers, Melvin H Friedman, and Jonathan M Nichols "*Introduction to Infrared and Electro-Optical Systems*," Second Edition. Friedman Jonathan Nichols, 2013

[8]J. S. Accetta, David L. Shumaker. *"The infrared and Electro-Optical Systems Handbook*". Infrared Information Analysis Center, Environmental Research Institute of Michigan, 1993

[9]Bahaa E. A. Saleh, Malvin Carl Teich, " *Fundamentals of Photonics*," John Wiley & Sons, Inc.1991

[10] A. Rogalski, K. Adamiec, and J. Rutkowski. "*Narrow-Gap Semiconductor Pho-todiodes*,". SPIE-The International Society for Optical Engineering, Bellingham,WA, 2000.

[11] Hansen G L, Schmit J L and Casselman T N, Energy gap versus alloy composition and temperature in $Hg_{1-x}Cd_xTe$ *J. Appl. Phys.* 53 7099 –10, 1982

